Regional deposition of the allergens and micro-aerosols in the healthy human nasal airways

Mohammad Hazeri [a], Mohammad Faramarzi [b], Sasan Sadrizadeh [c], Goodarz Ahmadi [d], Omid Abouali [a,*]

[a] *School of Mechanical Engineering, Shiraz University, Shiraz, Iran*
[b] *Department of Otolaryngology-Head & Neck Surgery, Shiraz University of Medical Sciences, Shiraz, Iran*
[c] *Department of Civil and Architectural Engineering, KTH University, Stockholm, Sweden*
[d] *Department of Mechanical & Aeronautical Engineering, Clarkson University, Potsdam, NY, USA*

A R T I C L E   I N F O

A B S T R A C T

The nasal cavity is the inlet to the human respiratory system and is responsible for the olfactory sensation, filtering pollutant particulate matter, and humidifying the air. Many research studies have been performed to numerically predict allergens, contaminants, and/or drug particle deposition in the human nasal cavity; however, the majority of these investigations studied only one or a small number of nasal passages. In the present study, a series of Computed Tomography (CT) scan images of the nasal cavities from ten healthy subjects were collected and used to reconstruct accurate 3D models. All models were divided into twelve anatomical regions in order to study the transport and deposition features of different regions of the nasal cavity with specific functions. The flow field and micro-particle transport equations were solved, and the total and regional particle deposition fractions were evaluated for the rest and low activity breathing conditions. The results show that there are large variations among different subjects. The standard deviation of the total deposition fraction in the nasal cavities was the highest for $5 \times 10^4 <$impaction parameter (IP)$< 1.125 \times 10^5$ with a maximum of 20%. The achieved results highlighted the nasal cavity sections that are more involved in the particle deposition. Particles with IP = 30,000 deposit more in the middle turbinate and nasopharynx areas, while for particles with IP = 300,000, deposition is mainly in the anterior parts (kiesselbach and vestibule regions). For small IP values, the amounts of deposition fractions in different regions of the nasal cavity are more uniform.

1. Introduction

One of the important functions of the human nasal cavity is its role in filtering airborne particles and delivering clean air to the lungs. Moreover, the nasal cavity is also important in the drug delivery process, as the therapeutic drugs could be delivered from the olfactory region to the brain. Extensive research studies have been carried out regarding the particle deposition in the human nasal cavity. However, the majority of these earlier studies were limited to a small number of subjects. Therefore, the detailed study of the nasal particle deposition, considering different subjects, is important.

---

* Corresponding author. School of Mechanical Engineering, Shiraz University, Shiraz, Iran.
E-mail address: abouali@shirazu.ac.ir (O. Abouali).

Many research studies have been conducted on the deposition of micro-particles in different regions of the human nasal cavity (Dastan, Abouali, & Ahmadi, 2014; Farhadi Ghalati et al., 2012; Ghahramani, Abouali, Emdad, & Ahmadi, 2017; Naseri, Abouali, Ghalati, & Ahmadi, 2014; Naseri, Shaghaghian, Abouali, & Ahmadi, 2017). With the increase in computational power, large numbers of nasal samples have been considered in recent studies to incorporate the impact of diversity in nasal anatomy but only on flow dynamics. These include both patient (Liu et al., 2012; Zhao et al., 2014) and healthy subjects (Borojeni et al., 2020; K. Wang, Denney, Morrison, & Vodyanoy, 2006; Zhao & Jiang, 2014). Golshahi and Hosseini (Golshahi & Hosseini, 2018) studied total particle deposition in the nasal cavity of infants, children, and adults experimentally and clinically.

The segmentation of the anatomical area in the nasal cavity is done for calculating the particle deposition. Typically, these segmentations have been made according to the importance of each part of the nasal cavity (which is based on the type of tissue, position or specific function of each region). These subdivisions should be anatomically definable and have clear boundaries between each region. Previous research efforts have provided different types of subdivisions to report particle deposition percentages (Dong, Ma, et al., 2018; Dong, Shang, Inthavong, Chan, & Tu, 2018; Ghahramani, Abouali, Emdad, & Ahmadi, 2014; Kiasadegh, Emdad, Ahmadi, & Abouali, 2020; Xi & Longest, 2008; Xi, Si, Kim, & Berlinski, 2011; Zhu, Lee, Lim, Lee, & Wang, 2011). The different definitions for the subdivisions have been used for the human olfactory region. The definitions in the earlier works are mostly based on the type of tissue and location of the epithelium. Due to anatomy differences, the area of the olfactory region may vary for each person. The location of the olfactory region is not accurately defined, and its position was qualitatively described within the nasal cavity (Dong, Ma, et al., 2018; Dong, Shang, et al., 2018; Xi & Longest, 2008; Zhu et al., 2011). There is an uncertainty in the literature of the field about the size of this region. For example, the size olfactory area is reported to be in the range of 1–10 cm^2 for each nasal passage (Arthur C. Guyton, 2016; Bear, Connors, & Paradiso, 2007; Leopold et al., 1995; López-Elizalde et al., 2018; Mark F.; Moran, Rowley, Jafek, & Lovell, 1982; Sahin-Yilmaz & Naclerio, 2011). Because of that, some researchers investigated the nano-particle deposition on this region assuming different sizes for the olfactory area (Garcia, Schroeter, & Kimbell, 2015), which showed a noticeable effect for a range of particle diameters. In the most detailed segmentation of the nasal cavity, the surface of the nasal airway has been divided into eleven anatomical sections, and the regional micro-particle deposition has been investigated for one human subject (Y. D. Shang, Inthavong, & Tu, 2015).

The gender, age and ethnicity might be the other reasons for difference in particle deposition in nasal cavity. Jaques and Kim (Jaques & Kim, 2000) investigated the effect of gender on particle deposition within the respiratory system of eleven men and women experimentally. The differences in the role of filtering of nasal cavity between children and adults were also studied and compared experimentally (Bennett, Zeman, & Jarabek, 2008; Borojeni, Noga, Vehring, & Finlay, 2014). In another study, differences in particle deposition fraction (DF) for the four African, Latin American, Asian, and white ethnicities were investigated using numerical simulations (Keeler, Patki, Woodard, & Frank-Ito, 2015). Even partial details of the nasal anatomy can affect the particle deposition. For example recent research studies have also investigated the effect of vestibule shape (presence or absence of notch) on particle deposition (Dong, Ma, et al., 2018). Also, in the numerical simulation of the nasal airway, it was found that the amount of surface smoothness has a significant effect on particle deposition (Schroeter, Garcia, & Kimbell, 2011). In addition, modeling the surrounding of the inlet of the nasal cavity provides a more accurate estimate for the particle deposition within the nasal cavity especially in vestibule area (Y. D. Shang, Dong, Inthavong, & Tu, 2015).

One of the main aims of present work is to find the details of the regional deposition of the allergens in the nasal cavity. Allergies are one of the most common diseases that affect many people around the world. In western countries, 10–30% of people have allergic rhinitis (Dykewicz & Hamilos, 2010). Allergens are of various types, and some of them stimulate the human's respiratory system and trigger the immune system to overreact. Allergens that trigger the human respiratory system can be in different sizes and types: environmental dust, mold, pet hair, and pollen (Dykewicz & Hamilos, 2010; Platts-Mills, 1998; Salvaggio, 1994). The diameter of pollen particles of flowers and trees is between 20 and 60 μm (Jeong, 2016), while cat allergens are less than 5 μm in diameter (Luczynska, Li, Chapman, & Platts-Mills, 1990). The actinomycete spores are ranged in 1 and 2 μm, and the dust particles are about 50 μm in diameter (Salvaggio, 1994). Allergen particles may deposit on different parts of the nasal cavity due to their size distribution. Thus, assessment of local deposition of allergen particles with different sizes for diverse individuals is important in targeted identification and treatment. In addition, recent severe COVID-19 pandemic requires a better understanding of the regional deposition of the inhaled particles through the nasal airway.

In our recent study (Hazeri, Farshidfar, Faramarzi, Sadrizadeh, & Abouali, 2020) the physiology, airflow pattern, and heat and moisture transfer in a group of ten Caucasian subjects with healthy nasal cavities including five adult males and five adult females ranging in age from 21 to 78 years, with normal vestibule was studied. In the present work, the total and the regional particle deposition for the same group were investigated. Considering right and left passages of ten healthy subjects, twenty nasal passages are available for evaluation of the total and local micro-particle deposition. The statistical analysis of the results provided a reliable representation of the micro-particle deposition in the nasal cavity of healthy subjects.

2. Method

2.1. Subjects

To investigate healthy subjects, from a large number of CT scan images taken in Dena Hospital (Shiraz, Iran) 10 image series were anonymously selected as normal subjects with the approval of a specialist. All the images had been acquired as a part of the routine clinical procedure in the hospital and they were available before starting the present project. All selected patients (the identities had been removed) had a healthy nasal cavity and their CT images had previously been taken for other problems such as sinus infections,

brain-related disorders, etc. All subjects with nasal septal deviation, turbinate hypertrophy, allergies, nasal polyps, atrophic rhinitis, and concha bullosa were excluded. The 3D geometry was developed for all nasal cavities. Earlier studies have shown that airflow and particle deposition in the sinuses of healthy subjects were very small (Bahmanzadeh, Abouali, & Ahmadi, 2016; Bahmanzadeh, Abouali, Faramarzi, & Ahmadi, 2015; Y. De Wang, Lee, & Gordon, 2012; O. Abouali, E. Keshavarzian, P. Farhadi Ghalati, A. Faramarzi, 2012). Hence, all sinuses were excluded in the computational domain of the present study.

2.2. Geometries construction

The separation of tissue and airway boundary was performed using Mimics 17.0 and the segmentation threshold in the range of −1024 to −300 HU was used for all the subjects in this study. The surfaces of all nasal passages were smoothed sufficiently to represent the presence of mucosa on the nasal cavity (Fig. 1). Segmentation of the nasal cavity surfaces was performed according to the anatomical location of each region. There are clear definitions for all parts except the olfactory region. There is uncertainty about the makeup of the olfactory area. Three different areas were defined for the olfactory region based on the data found in the earlier literature (Shang et al., 2015b; Arthur C. Guyton, 2016; Dong, Ma, et al., 2018; Gleeson & Clarke, 2008; Leopold et al., 1995; López-Elizalde et al., 2018; Mark F. Bear et al., 2007; Moran et al., 1982; Sahin-Yilmaz & Naclerio, 2011; Y. Shang, Dong, Inthavong, & Tu, 2015; Shang et al., 2015b; Suman, 2013) (Fig. 2). In this study, we investigate three earlier defined different sizes. The smaller surface, which is believed to have olfactory neurons, is located just under the olfactory bulb (under the cribriform plate in CT images) and is named as the smaller olfactory surface. The second assumed olfactory surface is a part of the nasal cavity that most references agree on and is more general (Per G. Djupesland, Messina, & Mahmoud, 2014; Per Gisle Djupesland, 2013; Mark F. Bear et al., 2007; Shi, Kleinstreuer, & Zhang, 2006; Suman, 2013; Xi, Zhang, & Si, 2015; Zhao et al., 2014). This is named as the medial olfactory surface in present work. The larger olfactory surface is also considered as the maximum area reported for the olfactory area in the nasal cavity. The sizes of these three projected surfaces are approximately 2.5, 5, and 10 cm^2 in each nasal passage, respectively. Other parts of the nasal cavity were also divided into regions named vestibule, kiesselbach, atrium, inferior, middle and superior turbinates, upper and lower septum, upper and lower maxilla, and the nasopharynx that are shown in Fig. 2.

2.3. Numerical method

After the reconstruction of geometries, the flow field and particle transport equations were solved numerically using the CFD-DPM method. The mass and momentum conservation equations were solved for resting and low activity breathing conditions (laminar airflow) and then particle transport equations were solved using Lagrangian approach. ICEM-CFD software package and ANSYS Fluent 18.0 were used for meshing and performing numerical simulation, respectively. Grid independence test was done to ensure that the results are independent of the grid size. For this purpose, an unstructured quadratic grid with 2.7 million cells was used for the external hemisphere which covers the exterior nose domain and a hybrid grid was used for the inside of the nasal cavity (consists of 4.6 million cells of quadratic elements and 7–9 layers of prism cells near the wall). The final size of the grid for the computational domain is 7.3 million. In addition, the independence of the simulation results for particle deposition fractions from the number of injected particles was investigated. Also, the maximum number of injected particles that have been used for small particles is 1.4 million. Details of grid generation, particle number study, and CFD-DPM method are given, respectively, in Appendices A, B and C.

(a). Reconstruction of 3d models　　　**(b).** Smoothed final domains
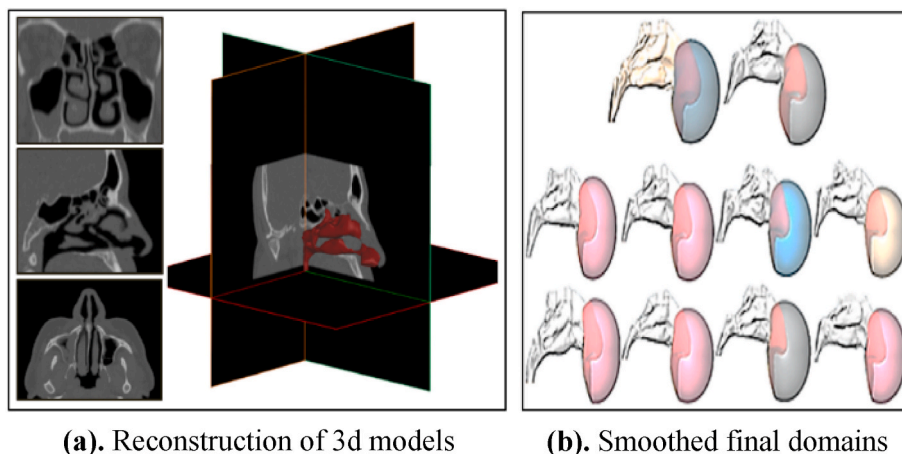
Fig. 1. Geometry construction. **(a)** Reconstruction of 3D models of the nasal cavity by a series of 2d CT images. **(b)** The 3D computational models of 10 healthy persons.

(a) Turbinate side view   **(b)** Septum side view
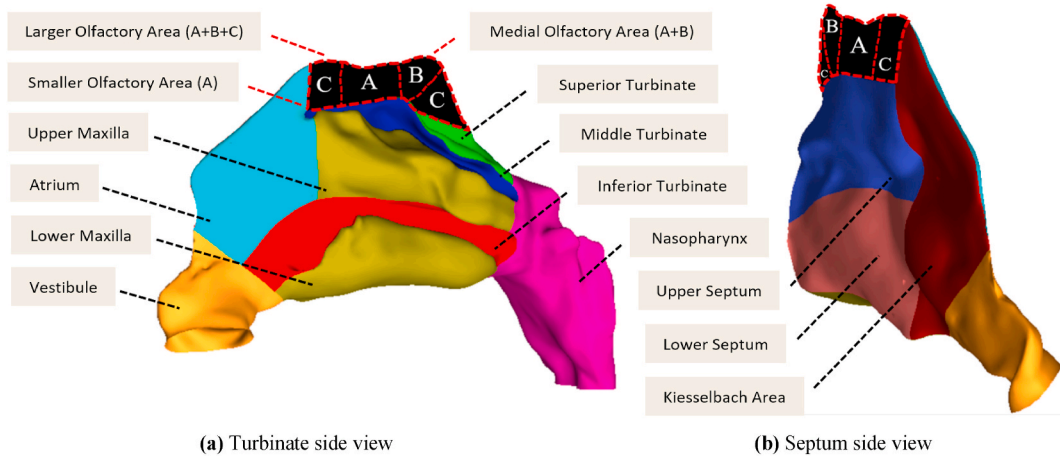
Fig. 2. Nasal cavity surface segmentation. **(a)** Turbinate side view contains: vestibule, atrium, olfactory area, the upper and lower part of the maxilla, superior, middle, and inferior turbinate and nasopharynx. **(b)** In the septum side view, the vestibule, kiesselbach area, the upper and lower part of the septum, and olfactory area can be observed.

2.4. Statistical analysis

Three kinds of Student's t-tests were used in this study. A one-sample *t*-test is used to test if a mean value of population is significantly different from a hypothesized value. Independent two-tailed Student's t-tests were used to identify the statistically significant change of the results for different subjects or different regions of the samples. Paired two-tailed Student's t-tests were used to test differences in the results for different breathing rates. Differences in results were considered significant when it represents about 95% of the population (p-values $\leq$ 0.05).

3. Results and discussion

Total and local micro-particle deposition for 20 normal nasal air passages of ten healthy subjects are investigated, and results are reported based on particle diameter and impaction parameter. The impaction parameter (IP) is defined as

$$\text{IP} \ (\mu m^2 cm^3 / s) = d_p^{\ 2}(\mu m^2) \times Q(cm^3 / s) \tag{1}$$

where d_p is the particle diameter, and Q is the breathing rate. The impaction parameter includes the influence of the main parameters that control the micro-particle deposition in the nasal cavity.

3.1. Total particle deposition

The total particle deposition fraction (DF) is defined as the number of particles deposited on the entire nasal airway surfaces divided by the number of inhaled particles. Variations of the DF versus particle diameter and impaction parameter are plotted in Fig. 3a and

(a) Total DF versus particle diameter   **(b)** Total DF versus impaction parameter   **(c)** Total unilateral DF versus Stokes parameter
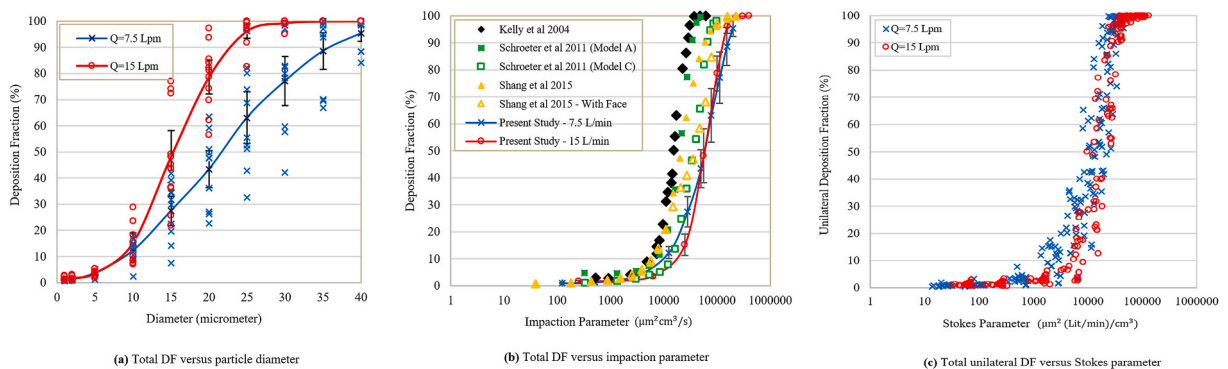
Fig. 3. Total micro-particle deposition fraction for both flow rates of 7.5 and 15 L/min (a) in ten studied nasal cavities versus particle diameter **(b)** average and SD versus impaction parameter compared with previous studies. **(c)** Unilateral deposition in 20 nasal passages versus Stokes number (Eq. (2)).

Fig. 3b, respectively. Here the micro-particle deposition percentages in the diameter range of 1–40 μm are evaluated. For breathing rates of 7.5 and 15 L/min, the total DF graphs are evaluated and are averaged over the 10 samples nasal airways, and the corresponded mean, and the standard deviation are shown in Fig. 3a and b (The length of the vertical line in this figure indicates the standard deviations of the data). The highest standard deviation of 20% of the deposition fraction data corresponds to 50,000 < IP < 112,500,
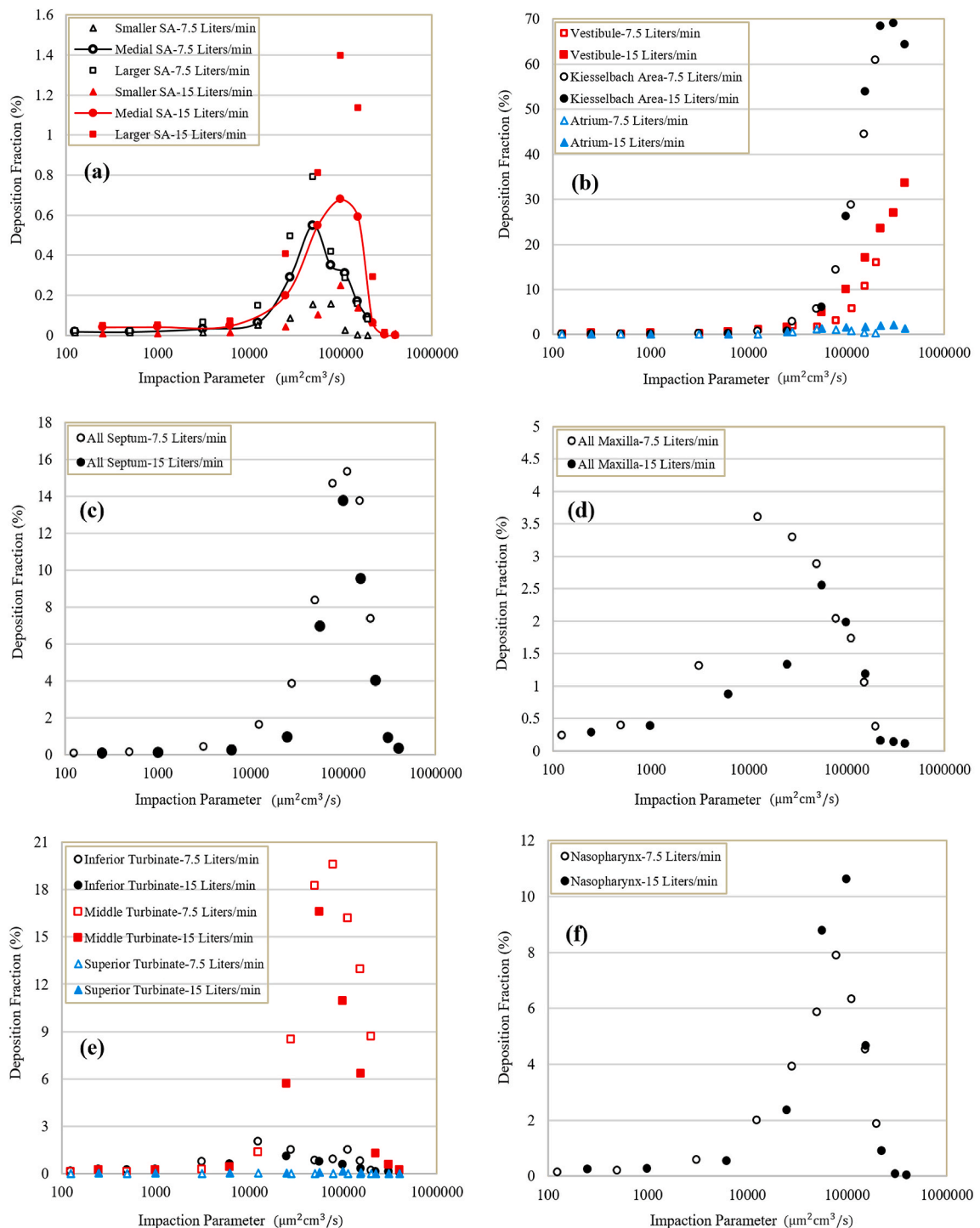

Fig. 4. Variation of micro-particle DF versus IP for different regions of the nasal airway for rest and low activity conditions. **(a)** Smaller, medial and larger olfactory surface. **(b)** Vestibule, kiesselbach area and atrium. **(c)** Septum wall. **(d)** Whole maxilla surface. **(e)** The inferior, middle and superior turbinates. **(f)** Nasopharynx.

which occurs for a diameter of 25 μm for the breathing rate of 7.5 L/min and for a diameter of 15 μm for the air flow rate of 15 L/min. For IP < 10,000 and IP > 200,000, the standard deviation is small. Also, as expected, more particle deposition occurs at higher breathing rates by increasing the particle inertia. However, the difference between the two flowrates is noticeable for the particle sizes between 15 and 35 μm (two-sample, paired *t*-test: p ≤ 0.037). For the particle sizes smaller than 10 μm, the difference between the DF for two flowrates is negligible.

It is seen that the results of the present study and other numerical solutions are significantly different from those of the experimental data of Kelly et al. (Kelly, Asgharian, Kimbell, & Wong, 2004). Schroeter et al. (Schroeter et al., 2011) attributed these differences to the low resolution of MRI images and the high roughness of the model used in the experiments by Kelly et al. (Kelly et al., 2004). Schroeter et al. (Schroeter et al., 2011) studied the effect of surface roughness on particle deposition. In Fig. 3b, the particle DFs for the two models of Schroeter et al. (Schroeter et al., 2011) (green squares) and the two models of Shang et al. (Y. D. Shang, Dong, et al., 2015) (yellow triangles) are reproduced for comparison. Shang et al. (Y. D. Shang, Dong, et al., 2015) studied the influence of including the external regions around the face on the predicted total deposition in the nasal airway. The results show both parameters, surface smoothness, and considering the effect of the region near the face, decrease the total particle DF. In the present study, the surfaces of all nasal samples were smooth, and the external region around the nose was included in the computational model. A combination of these two effects appears to lead to lower particle DF prediction in present work compared to those from earlier works (Kelly et al., 2004; Schroeter et al., 2011; Y. D. Shang, Dong, et al., 2015). As can be seen in Fig. 3b, IP reduced the data scatter for different flowrates (Fig. 3a) and the mean curves for two flowrates are close to each other.

Other parameters had been also used before to show the data of DF for different subjects and also various flow rates. Garcia et al. (Garcia, Tewksbury, Wong, & Kimbell, 2009) compared these different parameters and showed that the Stokes number defined based on equation (2) is an appropriate parameter to relate the inter-individual variability in total DF to some anatomical measurement. The same analysis was performed here for unilateral DF in twenty nasal passages of present work and the results are shown in Fig. 3c. The modified impaction parameter of $d^2 \Delta p^{2/3}$ can also play the same role and is an appropriate parameter. Other Stokes numbers based on other characteristic diameters (Volume$^{1/3}$ and volume/surface) were also tested but the data scatter was much higher compared to that for the used one here.

$$\text{Stk} = \text{IP}_{\text{Unilateral}} / d_c^3 = \left(d_p^2 \times Q_{\text{Unilateral}} \right) / d_c^3 \tag{2}$$

where $d_c = (0.0181 \times L_{\text{Nose}}/R_{\text{Unilateral}})^{4/19}$ and $R_{\text{Unilateral}} = \Delta p_{\text{Unilateral}}/Q_{\text{Unilateral}}^{1.75}$. L_{Nose} (cm) was defined as the linear distance from the nostrils to the end of the septum and the dimension of the R is Pa over mL/s.

3.2. Regional particle deposition

The primary purpose of this study is to investigate the regional particle deposition on different parts of the nasal cavity for ten different subjects. The local DF of particles in each region of the nasal cavity varies with particle diameters and breathing rates. For this purpose, the results of the regional deposition of micro-particles in 20 healthy nasal air passages are evaluated and reported in this section.

Olfactory area: The olfactory area is a very important part of the nose for sensing smell and in the process of drug delivery to the brain. Hence, based on the definitions in earlier studies, three different regions representing the olfactory area (smaller, medial and larger surfaces) were selected for each person. The averages of regional micro-particle depositions in the olfactory region of the twenty studied nasal passages are presented in Fig. 4a. Additional details of the computed standard deviation of the data are reported in Table 1. This figure shows that the graphs for different flow rates are not similar despite using the IP for the horizontal axis. This means that the impaction is not the main mechanism for deposition of particles in this region. The olfactory cleft is a narrow and small duct (with about 1–2 mm width) located above the main airway and the airflow does not pass through that directly. Also, the deposition fraction in the olfactory region is generally quite low. The maximum DF in the largest size olfactory region for all studied subjects is 1.4 percent (with a standard deviation of 1.8%). Olfactory DF is generally more pronounced in the range of 25,000 < IP < 100,000. The

Table 1
Average and Standard deviation of regional DF percentage for olfactory area.

d(μm)	Smaller olfactory SA		Medial olfactory SA		Larger olfactory SA	
	Q = 7.5 Lpm	Q = 15 Lpm	Q = 7.5 Lpm	Q = 15 Lpm	Q = 7.5 Lpm	Q = 15 Lpm
1	0.01 ± 0.01	0.01 ± 0.01	0.02 ± 0.02	0.04 ± 0.05	0.02 ± 0.02	0.05 ± 0.06
2	0.01 ± 0.02	0.01 ± 0.01	0.02 ± 0.01	0.04 ± 0.06	0.02 ± 0.02	0.05 ± 0.06
5	0.01 ± 0.02	0.01 ± 0.01	0.03 ± 0.03	0.05 ± 0.05	0.06 ± 0.06	0.07 ± 0.07
10	0.05 ± 0.05	0.04 ± 0.06	0.06 ± 0.04	0.2 ± 0.24	0.15 ± 0.22	0.41 ± 0.54
15	0.08 ± 0.11	0.1 ± 0.16	0.29 ± 0.41	0.55 ± 1.3	0.49 ± 0.58	0.81 ± 1.4
20	0.15 ± 0.28	0.25 ± 0.38	0.55 ± 0.85	0.68 ± 0.92	0.79 ± 0.96	1.4 ± 1.8
25	0.16 ± 0.3	0.14 ± 0.23	0.35 ± 0.53	0.59 ± 1.0	0.42 ± 0.59	1.1 ± 1.9
30	0.03 ± 0.09	0.06 ± 0.21	0.31 ± 0.96	0.06 ± 0.22	0.29 ± 0.93	0.29 ± 1.0
35	0 ± 0.01	0.01 ± 0.03	0.17 ± 0.5	0 ± 0.01	0.16 ± 0.49	0.01 ± 0.05
40	0 ± 0	0.01 ± 0.02	0.09 ± 0.34	0 ± 0	0.08 ± 0.33	0 ± 0

data in Table 1 shows that the maximum particle DF percentage in the olfactory region occurs for the size range of 15–25 μm, and the highest DF is seen for the diameter of 20 μm. At larger diameters, the particles are not able to reach the olfactory region due to their high inertia and deposition in the earlier regions of the nose. The smaller particles are more likely to move along the airflow streamlines and do not deposit in the olfactory region. As the flow rate increases, the particle DF increases as well. To increase the DF in the olfactory region, a higher breathing rate is needed combined with particles in size range of 15–25 μm. For this diameter range, by doubling the airflow rate, the percentage of particles DF in the medial olfactory region increases by about 60%.

Fig. 4a shows large differences in the particle DF depending on the size of the olfactory region. Differences between large and medial olfactory regions were statistically significant for particles equal to or smaller than 20 μm (two-sample, paired t-test: $p \leq 0.034$). Generally, what we defined as the medial olfactory region is more popular (Per G. Djupesland et al., 2014; Per Gisle Djupesland, 2013; Mark F. Bear et al., 2007; Shi et al., 2006; Suman, 2013; Xi et al., 2015; Zhao et al., 2014) and is typically used to represent the percentage of olfactory DF for healthy people. Considering this region and diameter range, the average percentage of micro-particle deposition in the human olfactory region is, respectively, 0.4 percent (with SD of 0.6 percent) and 0.6 percent (with SD of 0.8 percent) for the flow rates of 7.5 and 15 L/min. The maximum of the mean deposition in the olfactory region among the twenty nasal passages for 20 μm diameter is 0.68% (with SD of 0.92%). As using the nasal route is one way for drug delivery to the brain by administering the deposition of drugs at the olfactory region, the amount of particle deposition in this region is important. For example, Xi et al. (2015, 2016) investigated the enhancement of the particle deposition in the olfactory region using a magnetic field (Xi et al., 2015; Xi, Zhang, Si, Yang, & Deng, 2016). In addition, it should be noted that the results for the drugs injected by a spray might be different from present work as the effect the spray on the flow field has not been considered in present work.

Vestibule: The first part of the human nose that includes the nostrils is the vestibule region, which plays an important role in capturing large inhaled particles. As the main mechanism for deposition in this region is inertia impaction, Fig. 4b shows that the mean DF in the vestibule region increases as the IP increases. This figure also shows that the DF for both breathing rates of 7.5 and 15 L/min versus IP are roughly the same. The average and standard deviation of the DF for both flow rates based on the particle diameter are also listed in Table 2. For particles smaller than 10 μm, the particle DF in the vestibule is negligibly small, and the smaller size particles enter the inner parts of the nasal cavity. However, for particles larger than 15 μm, the role of this region in filtering the particles becomes more pronounced. As the particle diameter increases to 40 μm, for flow rates of 7.5 and 15 L/min, the means of DF percentage reach to 16.1 and 33.5, and the corresponding variances are 19% and 22% respectively. That is, by doubling the breathing rate (increasing the airflow momentum), the particle DF increases proportionally, and the role of the vestibule region in capturing the inhaled air increases. Vestibule DF is seen to be higher than all other nasal regions, except for the kiesselbach area, for particles with IP $> 225,000$ (two-sample, independent t-test: $p \leq 0.002$).

Kiesselbach area: This area is located next to the vestibule, where the five arteries intersect on the septum. Like other parts of the nasal cavity, the task of the kiesselbach region is warming and humidifying the inhaled air, but the particular importance of this region is its large number of blood vessels and also high capturing rate of particles. It is worth mentioning that the majority of nose bleeding occurs in the kiesselbach area due to the rich vascular supply and susceptibility of injury in this area (Gleeson & Clarke, 2008). In our previous study, it was observed that the kiesselbach area also had a high value of wall shear stress and a significant role in warming the inhaled air (Hazeri, Farshidfar, Faramarzi, Sadrizadeh, & Abouali, 2020). As shown in Fig. 4b and Table 2, the particle DF in this area is continuously increasing with the IP for a flow rate of 7.5 L/min, but for the flow rate of 15 L/min, the DF has a maximum. This is because the vestibule captures a lot of large particles, and a smaller number of large particles get to this area. Another interesting point is the high percentage of particle DF in this area. For IP$\geq 2 \times 10^5$, more than 50% (one sample, t-test: $p \leq 0.022$) of the particles passing through the nasal nares are deposited within the Kiesselbach area. For large particles with IP $> 100,000$, the DF of this region is higher than other regions of the nasal cavity (two-sample, independent t-test: $p \leq 0.06$). Therefore, this region has a very high DF rate and is a very important site in the nasal cavity in the micro-particle deposition process larger than 20 μm.

Atrium: This region is located on the lateral side of nasal passage, between vestibule and turbinates. The variation of the average DF versus IP in the atrium region is also shown in Fig. 4b and the corresponding average and standard deviation are presented in Table 2. While atrium is located just in front of the Kiesselbach area, the DF percentage for this region is much lower than other regions in the anterior part of the nasal cavity (vestibule and kiesselbach area) for IP$\geq 10^5$ (two-sample, independent t-test: $p \leq 0.03$). The peak

Table 2
Average and Standard deviation of regional DF percentage for vestibule, atrium and kiesselbach area.

d(μm)	Vestibule		Atrium		Kiesselbach area	
	Q = 7.5 Lpm	Q = 15 Lpm	Q = 7.5 Lpm	Q = 15 Lpm	Q = 7.5 Lpm	Q = 15 Lpm
1	0.2 ± 0.13	0.31 ± 0.22	0.01 ± 0.02	0.05 ± 0.06	0.03 ± 0.02	0.06 ± 0.04
2	0.21 ± 0.12	0.33 ± 0.25	0.01 ± 0.02	0.05 ± 0.06	0.04 ± 0.02	0.06 ± 0.05
5	0.38 ± 0.26	0.62 ± 0.61	0.02 ± 0.02	0.07 ± 0.1	0.15 ± 0.08	0.13 ± 0.11
10	1.3 ± 0.88	1.6 ± 1.5	0.11 ± 0.12	0.57 ± 1.6	0.7 ± 0.54	0.73 ± 0.78
15	2.1 ± 2.1	4.9 ± 6.9	0.56 ± 1.8	1.3 ± 4	2.8 ± 2.9	6 ± 9
20	1.8 ± 2.6	10 ± 12	1.2 ± 4.9	1.6 ± 3.2	5.6 ± 6.5	26.2 ± 21
25	3.2 ± 5.7	17 ± 19	1.1 ± 4.7	1.7 ± 5.3	14.3 ± 14.8	53.8 ± 21
30	5.9 ± 9.2	23.5 ± 24	0.86 ± 3.4	1.9 ± 8.2	28.7 ± 24	68.4 ± 18
35	10.9 ± 14	27 ± 21	0.46 ± 2.1	2.1 ± 8.4	44.3 ± 28	68.9 ± 20
40	16.1 ± 19	33.5 ± 22	0.28 ± 1.3	1.4 ± 5.4	60.8 ± 22	64.3 ± 22

DF percentage for atrium region for breathing rate of 7.5 L/min is 1.2% and occurs for larger particles with an IP of 50,000. Similarly, for a flow rate of 15 L/min, the peak mean DF is 2.1% and occurs at IP = 306,250. Due to the small number of particle deposition in the atrium, the corresponding standard deviations are quite high for this region and are 8.4% and 4.9%, respectively, for the two noted breathing rates.

Septum: The nasal septum divides the nasal cavity into two separate passages. Septum wall increases the total mucosal surface area in the nasal cavity. As it was mentioned before the Kiesselbach area was excluded from the septum in present work (Fig. 2b) and the particle deposition in this area was reported separately Fig. 4b. The septum wall is divided by the horizontal part of the middle meatus into the upper and lower parts regarding the location of the middle meatus. The summation of the mean deposition in both parts of the septum is shown in Fig. 4c versus IP and the average and standard deviation of DF versus particle diameter for each part of the septum are presented in Table 3. Fig. 4c shows that the DFs versus IP for both flow rates have the same trend and almost the same values, which indicates that the inertial impaction is the primary deposition mechanism in this region. For a breathing rate of 7.5 L/min, the maximum mean DF in the entire septum region is 15.3% and occurs for the 30 μm particles. Here the standard deviation is quite high and is about 19%. By increasing the airflow rate to 15 L/min, the maximum mean DF is 13.3% that occurs for 20 μm particles. For this breathing rate, the corresponding SD is 13%. According to Table 3, for higher flow rates, the deposition fractions in the upper part of the septum are much higher than those in the lower part for particle diameters of 10–20 μm (two-sample, independent t-test: p $\leq$ 0.028). The DF in the entire septum has the highest value at IP of about 100,000, as is seen in Fig. 4c.

Maxilla: The interface of the nasal airway surface with the maxillary sinus wall is defined as the maxilla. This section is divided into upper and lower parts. The upper and lower maxilla regions are the lateral side of the middle and inferior meatus, respectively. The mean of the DF in the entire maxilla versus IP is shown in Fig. 4d. According to this figure, the maximum of the mean DF for the flow rate of 7.5 L/min occurs at IP = 10,000, but for the flow rate of 15 L/min, the maximum occurs at an IP, which is almost one order of magnitude higher. At lower flow rate, the total DF on both maxilla surfaces reaches 3.6% (with SD of 2.3%), while at the higher flow rate, DF decreases to 2.5% with a standard deviation of 3.6%. In general, despite the large surface area of the maxilla, the amount of DF in this region is low. However, this region had the highest DF between all the regions for lower impaction parameter of $3.125 \times 10^3 < IP < 1.25 \times 10^4$ (two-sample, independent t-test: p $\leq$ 0.12).

Turbinates: Turbinates are internal structures within the nasal cavity whose primary function is to increase heat transfer and to moisturize the inhaled air and to remove the inhaled particles by increasing the mucous surface. Our earlier study showed that about 25.7% of the total nasal heat transfer occurs at the turbinates (Hazeri, Farshidfar, Faramarzi, Sadrizadeh, & Abouali, 2020). Typically, there are three turbinates on each side of the nasal cavity (rarely four), which are located on lateral nasal cavity walls.

Fig. 4e shows the variations of the DF in the superior, middle, and inferior turbinate regions. The results for average and the standard deviation of DF of the studied twenty nasal passages on these three turbinates are also presented in Table 4. The superior turbinate is much smaller than the middle and inferior turbinates and has a very low particle DF. For a breathing rate of 7.5 L/min, the DF in the superior turbinate is negligible (roughly zero), and for the flow rate of 15 L/min, the maximum DF was 0.16% with a standard deviation of 0.36%. In general, the DF in the middle turbinate is much higher than that for the inferior turbinate for a wide range of $2.5 \times 10^4 < IP < 2 \times 10^5$ (two-sample, independent t-test: p $\leq$ 0.014). This is because the middle turbinate directly faces the air entering the main airway. The maximum DF of 2% (SD = 1.4%) on the inferior turbinate occurs for 10 μm particles at a breathing rate of 7.5 L/min, and the peak is 1.1% (SD = 0.95%) for the flow rate of 15 L/min.

When the airflow rate (flow momentum) increases, the flow approaches with higher velocity to the Kiesselbach area and the middle turbinate. As the breathing rate increases, the particle DF on the middle turbinate increases for particle diameter smaller than 15 μm (two-sample, paired t-test: p $\leq$ 0.017), but the trend is reversed for larger particles (two-sample, paired t-test: p $\leq$ 0.048). The diameter for which the maximum DF in the middle turbinate region occurs depends on the airflow rate. For a flow rate of 7.5 L/min, the maximum DF is 18.3% (SD = 11%) which corresponds to the 25 μm particles, while for the flow rate of 15 L/min, the maximum DF is 16.6% (SD = 7.2%) for 15 μm particles. In Fig. 4e, it is seen that the maximum deposition for both flowrates occurs at the same IP value, and the overall trend of the graph is the same. In general, the amount of micro-particle DF in the middle turbinate area is much higher compared to other inferior and superior turbinate regions in the range of 56,250 > IP > 25,000 (two-sample, independent t-test: p $\leq$ 0.024). This is important when the regional depositions of the allergens and the inhaled drug are of interest.

Table 3
Average and Standard deviation of regional DF percentage for maxilla and septum.

| d(μm)	Lower Septum		Upper Septum		Lower Maxilla		Upper Maxilla	
	Q = 7.5 Lpm	Q = 15 Lpm	Q = 7.5 Lpm	Q = 15 Lpm	Q = 7.5 Lpm	Q = 15 Lpm	Q = 7.5 Lpm	Q = 15 Lpm
1	0.03 ± 0.02	0.03 ± 0.03	0.04 ± 0.02	0.07 ± 0.05	0.16 ± 0.21	0.11 ± 0.09	0.07 ± 0.07	0.18 ± 0.16
2	0.05 ± 0.03	0.04 ± 0.03	0.05 ± 0.03	0.07 ± 0.05	0.31 ± 0.41	0.18 ± 0.13	0.08 ± 0.06	0.2 ± 0.16
5	0.21 ± 0.12	0.1 ± 0.07	0.19 ± 0.11	0.15 ± 0.1	1 ± 0.86	0.55 ± 0.35	0.26 ± 0.24	0.32 ± 0.21
10	0.74 ± 0.49	0.25 ± 0.2	0.84 ± 0.43	0.66 ± 0.74	2.7 ± 1.8	0.59 ± 0.67	0.92 ± 0.86	0.74 ± 0.5
15	2.2 ± 2.1	0.77 ± 1.1	1.6 ± 1.2	5.9 ± 8.9	2.6 ± 3.3	0.24 ± 0.49	0.73 ± 1.1	2.3 ± 3.5
20	4.3 ± 5.6	2.5 ± 2.8	3.9 ± 3	10.8 ± 12	1.8 ± 2.6	0.15 ± 0.49	1.1 ± 2.6	1.8 ± 5
25	6.2 ± 6.4	3.8 ± 4.2	8.3 ± 7.4	5.8 ± 5.9	1.3 ± 3	0.12 ± 0.47	0.78 ± 1.7	1.1 ± 3.3
30	6.4 ± 6.4	2.7 ± 3.3	8.9 ± 15	1.5 ± 1.9	0.7 ± 2.5	0.03 ± 0.1	1 ± 3.2	0.12 ± 0.47
35	8 ± 9.3	0.45 ± 1.1	6.4 ± 10	0.44 ± 1	0.6 ± 2.3	0 ± 0.02	0.45 ± 1.2	0.13 ± 0.44
40	6.3 ± 9.2	0.2 ± 0.63	1.4 ± 3.2	0.12 ± 0.28	0.23 ± 0.72	0 ± 0.01	0.15 ± 0.62	0.1 ± 0.33

Table 4

Average and Standard deviation of regional DF percentage for turbinates and nasopharynx.

$d(\mu m)$	Inferior turbinate		Middle turbinate		Superior turbinate		Naso-pharynx	
	Q = 7.5 Lpm	Q = 15 Lpm	Q = 7.5 Lpm	Q = 15 Lpm	Q = 7.5 Lpm	Q = 15 Lpm	Q = 7.5 Lpm	Q = 15 Lpm
1	0.14 ± 0.16	0.23 ± 0.11	0.1 ± 0.07	0.21 ± 0.18	0.01 ± 0.01	0.02 ± 0.02	0.14 ± 0.06	0.23 ± 0.14
2	0.21 ± 0.19	0.25 ± 0.11	0.11 ± 0.08	0.23 ± 0.2	0 ± 0.01	0.02 ± 0.02	0.19 ± 0.08	0.26 ± 0.14
5	0.74 ± 0.41	0.59 ± 0.28	0.23 ± 0.14	0.38 ± 0.29	0 ± 0.01	0.02 ± 0.02	0.58 ± 0.26	0.53 ± 0.26
10	2 ± 1.4	1.1 ± 0.95	1.3 ± 0.93	5.7 ± 5.8	0 ± 0.01	0.02 ± 0.03	2 ± 0.93	2.4 ± 1.6
15	1.5 ± 1.8	0.74 ± 0.95	8.5 ± 6.5	16.6 ± 7.2	0 ± 0.01	0.07 ± 0.18	3.9 ± 3.3	8.8 ± 5.5
20	0.81 ± 1	0.54 ± 1.1	18.3 ± 11	10.9 ± 9.8	0 ± 0	0.16 ± 0.36	5.9 ± 3.1	10.6 ± 7.8
25	0.88 ± 2	0.3 ± 0.59	19.6 ± 12	6.3 ± 7	0 ± 0.01	0.07 ± 0.22	7.9 ± 3.1	4.7 ± 6.7
30	1.5 ± 3.8	0.1 ± 0.35	16.2 ± 14	1.3 ± 2.7	0 ± 0	0 ± 0	6.3 ± 2.4	0.89 ± 1.6
35	0.79 ± 2.3	0.09 ± 0.35	12.9 ± 17	0.55 ± 1.4	0 ± 0	0 ± 0	4.5 ± 7.8	0.08 ± 0.15
40	0.18 ± 0.5	0.07 ± 0.31	8.7 ± 14	0.22 ± 0.56	0 ± 0	0 ± 0	1.9 ± 3.6	0.03 ± 0.06

Nasopharynx: The nasopharynx begins at the end of the turbinates, where the two nasal passages merge and end at the beginning of the oral pharynx. This part of the nose is the last part of the nasal cavity in the filtration process of inhaled particles. According to Fig. 4f, particles with IP of around 100,000 (diameter of 15–30 μm for the studied breathing rates) have more chance to be captured in this region. Fig. 4f shows that the two DF graphs for 7.5 and 15 L/min have the same trend and have nearly the same values indicating that the primary deposition mechanism is the inertial impaction. The maximum DF for both flow rates occurs at IP = 100,000. These maxima are 7.9% (SD = 3.1%) for 7.5 L/min and 10.6% (SD = 7.8%) for 15 L/min. Therefore, for target drug delivery to the nasopharynx region, using particles with an IP of 100,000 is recommended.

The results show which region of a healthy nasal cavity has a greater role in capturing different sizes of inhaled particles. These findings may find applications for targeted drug delivery to a specific location in the nasal cavity. That is, it is possible to identify the particle IP value that is most effective in the deposition in a specific region of the nose. Also, Fig. 4 indicates which part of the nasal cavity is more influenced by inhaling allergen particles. For example, particles with IP = 30,000 deposit more in the middle turbinate and nasopharynx areas, while for particles with IP = 300,000, deposition is mainly in the anterior parts (kiesselbach and vestibule). For particle sizes and breathing conditions with small IP values, the amounts of deposition fractions in different regions of the nasal cavity are more uniform. As the IP increases, the differences in the DF in different regions of the nasal cavity become more noticeable. The vestibule and kiesselbach areas located at the beginning of the nasal cavity had very high DFs for the IP > 55,000.

In this section, we divided the nasal airway into larger parts: anterior (nostril to tip of turbinate), upper region (olfactory area and
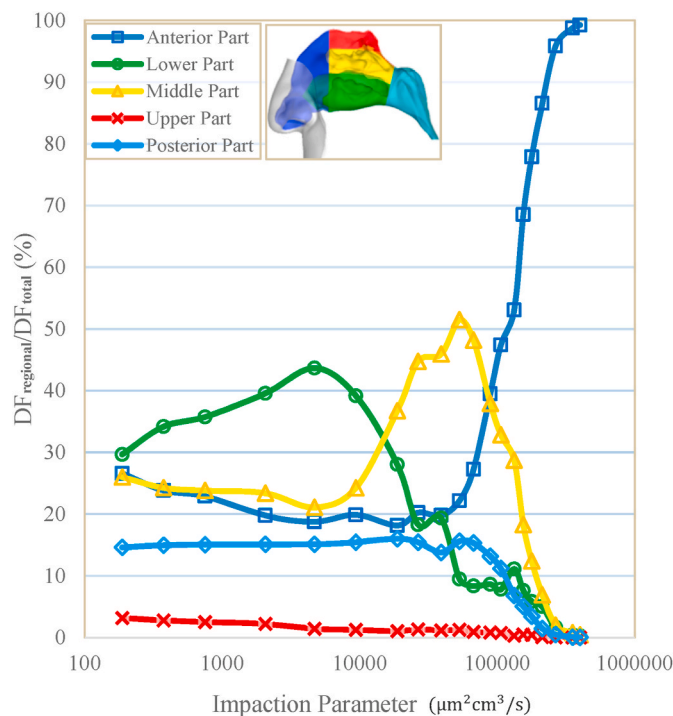
Fig. 5. Variation of regional DF normalized by total DF versus IP for the anterior, upper, middle, lower and posterior of the nasal cavity. (averaged for both studied flow rates).

superior turbinate), middle region (middle turbinate and upper septum and maxilla), lower region (inferior turbinate and lower septum and maxilla), and posterior region (nasopharynx) (See inset of Fig. 5). Variations of the regional DFs normalized by the total nasal DF ($DF_{regional}/DF_{total}$) are evaluated and the results are shown in Fig. 5. This figure shows that the portion of the anterior part from total DF mostly increases as IP increases, and the rate of increase becomes quite rapid for IP > 60,000. While the upper region contribution from total DF, which is quite low, decreases with the increase of the IP. The peak value of Fig. 5 for the lower region occurs at IP ≅ 5,000, while the peak value in the middle region occurs at IP ≅ 50,000. These findings show which part of the nasal cavity was more affected for different IP ranges of allergens. Fig. 5 also shows that the pattern of variation in DF of the vestibule and kiesselbach area is quite similar to the trend of the total particle deposition in Fig. 3b; hence, the process of particle transport within the entire nasal cavity is strongly influenced by the anterior part of the nasal cavity.

As the final point, a comparison is presented between the total deposition fractions of male and female subjects. Fig. 6 shows that for five adult males and five adult females studied in the present work, there are no noticeable differences between the mean total DF graphs between males and females for both flow rates (two-sample, independent *t*-test: p ≤ 0.94 for 7.5 and p ≤ 1 for 15 L/min). However, there are noticeable differences between the regional DFs between these two groups, which is not discussed here for the sake of brevity. All the data, including total and regional DF for all the ten subjects studied in this paper, are presented in an excel file that can be found in the supplementary file of the paper.

4. Conclusions

In the previous studies, total and regional particle depositions were obtained for a small number of samples. The present study evaluated the total and the regional micro-particle deposition for 20 nasal passages of 10 healthy subjects for the rest and low activity conditions. The average and standard deviation of the total and regional DF are computed, and the effects of intersubject variation of the nasal anatomy on the velocity field and DF percentage in the nasal cavity were assessed. The maximum of the standard deviation of the total micro-particle DF was 20%, which occurs in the range of 50,000 < IP < 112,500. This deviation was much lower for lower and higher impaction parameters.

Due to the importance of regional particle deposition, the nasal cavity surface was divided into different anatomical parts, and the regional DF results were evaluated. The presented results showed that the anterior region of the nasal cavity (from the nostrils to start of turbinates) plays a significant role in capturing large particles. In particular, the Kiesselbach and vestibule areas are highly effective in filtering large particles. In the inner part of the nasal cavity, more deposition occurs on the middle turbinate compared to the inferior turbinate. The DF on the septum wall (excluding the kiesselbach area) also is comparable to the middle turbinate. The maximum DF for the nasopharynx is around 10.6 ± 7.8% for the particles with IP roughly equal to 100,000.

The maximum DF of 1.4% in the olfactory region occurs in the IP of 100,000. For the largest size of the olfactory area, the corresponding regional deposition fraction of 20 μm particles is estimated to be 1.4 percent, with a standard deviation of 1.8%.

The kiesselbach area had the highest deposition rate compared to the other parts of the nasal airway for large particles with IP > 100,000 or diameters larger or equal to 30 μm. The DF in the vestibule region for particles with IP > 225,000 by the second highest after the kiesselbach area. Also, the middle turbinate region more effective in capturing the inhaled particles compared with the inferior turbinate area for a wide range of particle size with $2.5 \times 10^4 < IP < 2 \times 10^5$. The highest DF for the nasopharynx region occurs
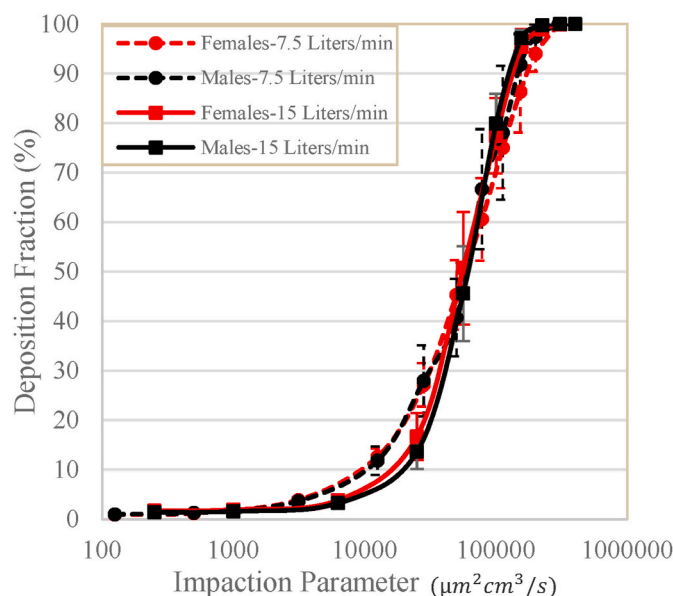

Fig. 6. Total micro-particle deposition fraction differences between males and females.

in a diameter range of 10–20 μm (IP = 100,000).

The presented results identified the IP for maximum regional deposition in the nasal cavity. This information may find application to targeted drug delivery to a specific location in the nasal cavity. In addition, the results suggest that cat allergens smaller than 5 μm (IP ≤ 6000) deposit in all parts of the nasal cavity but mostly in the lower part. Dust particles larger than 40 μm (IP ≥ 200,000) are captured by the anterior part of the nasal cavity. Fungal spores that are around 15 μm diameter are mainly deposited in the middle part (middle turbinate).

Data availability

A wide range of calculated data, including the total and regional deposition fractions of the nasal airways and different anatomical regions for all subjects, are available in a supplementary excel file attached to this paper.
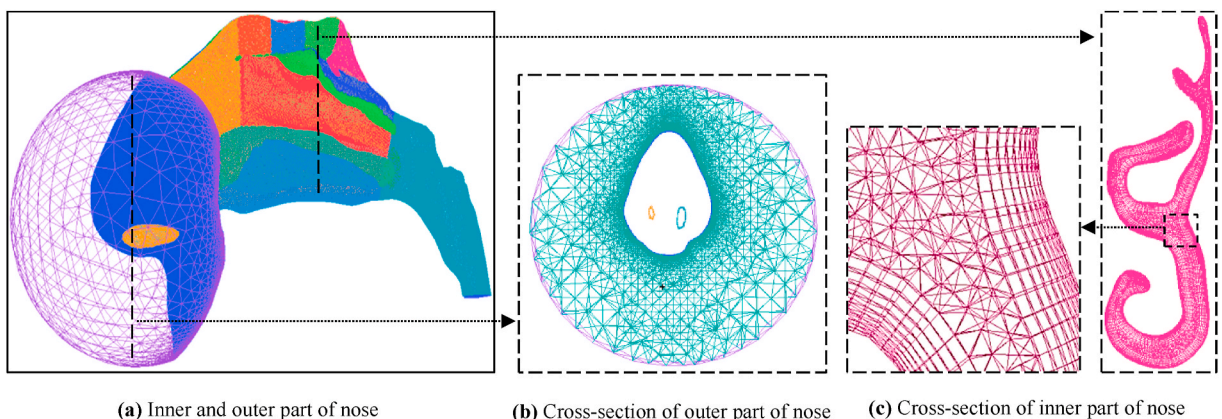
Declaration of competing interest

All the authors declare that there is no potential conflict of interest including any financial, personal or other relationships with other people or organizations within that could in appropriately influence (bias) this work.
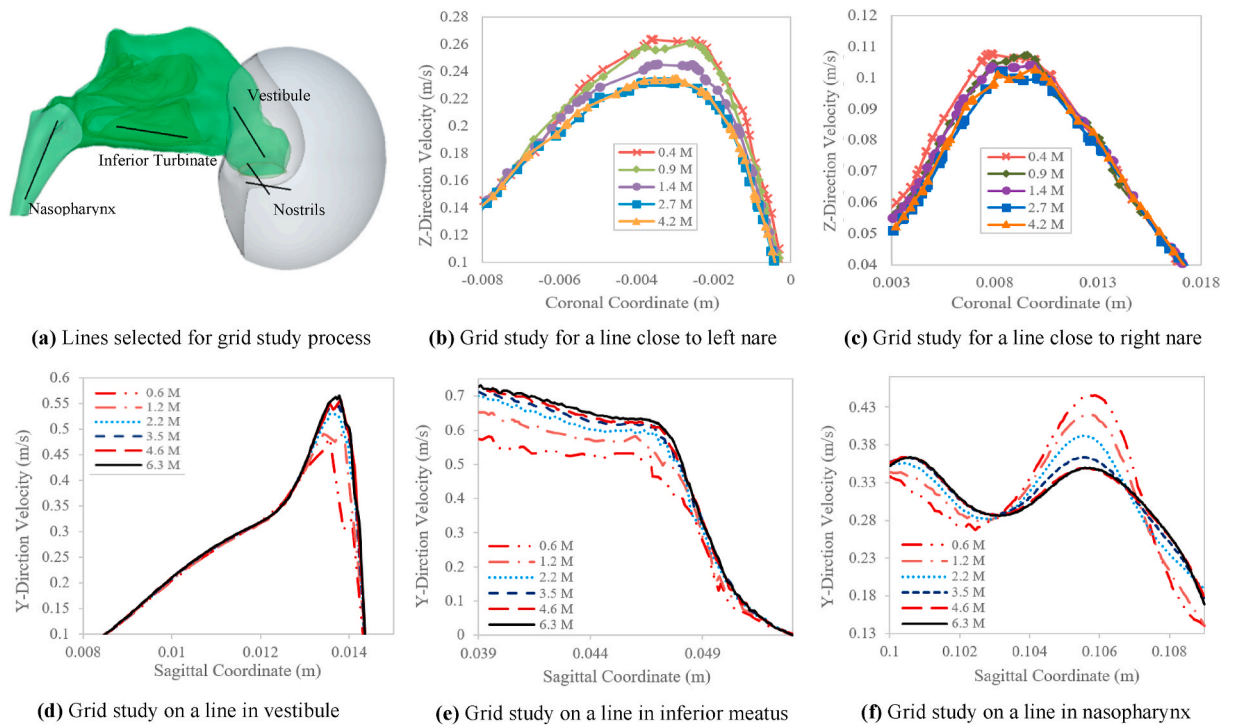
Appendices.

Appendix A: grid study

For grid study, the computational domain was divided into the outer and inner parts of the nose. In the surrounding outer area (outside the nasal cavity), an unstructured tetrahedral grid with 2.7 million tetrahedral cells was used (Fig. A1b). When a finer grid was used, the difference in the velocities under the nostrils was only 0.5% (Fig. A2b, A2c). Inside of the nasal cavity, a hybrid grid was used for calculating the velocity field in the boundary layer accurately. In this region near the walls, a finer structured grid (prism layer) was employed, and in the internal part of the nasal cavity, the tetrahedral elements were used (Fig. A1c). In order to perform the grid sensitivity study for the region inside of the nasal cavity, the changes in velocity with an increase of the grid size were studied for the grid in the inner part, and for the number of the prism layers close to the boundary. In addition, the variations of the particle DF for different grids are studied. For the inside of the nasal cavity, different grid sizes of 1.2, 2.2, 3.5, 4.6, and 6.3 million cells were tested, and a grid size of 4.6 million was selected. For the internal nose domain, velocity components at three lines in vestibule, inferior meatus and nasopharynx were compared for different grid sizes. This grid led to the results for velocity that differ less than 1% compared to the finer grid 6.3 million cells (Fig. A2d, A2e, A2f). To study the independency of the solution from the number and size of the prism layers, 3 to 15 layers with the height of the first layer in the range of 0.32 to 0.02 mm were studied. In this process, the total deposition fraction of particles was calculated for three different particle diameters and difference in DF is reported in percent with increase in number of layers or decrease in the height the first prism layer adjacent to the wall. As shown in Table A, DF is more sensitive to the height of the first prism layer. The results showed that using 7 to 9 layers of the prisms near to the nasal cavity walls with the height of 0.06 mm for the first layer and the growth ratio of 1.2 for the next layers leads to less than 1.5% difference for the deposition fraction of particles compared to that in a grid with a finer prism size.

(a) Inner and outer part of nose **(b)** Cross-section of outer part of nose **(c)** Cross-section of inner part of nose

Fig. A1. Grid generation. **(a)** Surface grid of domain, including inner and outer parts of the nose. **(b)** Cross-section of the outer part of the nose with the tetrahedral grids with a finer grid near the nose. **(c)** Hybrid mesh in cross-section of the right chamber of the nasal cavity using the tetrahedral elements and prism meshing near to the nasal cavity walls.

(a) Lines selected for grid study process   **(b)** Grid study for a line close to left nare   **(c)** Grid study for a line close to right nare

(d) Grid study on a line in vestibule   **(e)** Grid study on a line in inferior meatus   **(f)** Grid study on a line in nasopharynx

Fig. A2. Details of tetrahedral grid study. **(a)** Five selected lines in internal and external nose domains for grid study **(b),(c)** Grid study of external nose domain on two lines under nostrils. **(d),(e),(f)** Grid study of internal nose domain on three lines in vestibule, inferior meatus and nasopharynx, respectively.

Table A
Effect of number of layers and initial height of prism layer on total DF changes (Error values were obtained compared to the lower initial height and higher number of layers, Err $= |DF_n-DF_{n+1}|/DF_{n+1}$ which n refers to the row of table)

Initial height's effect		Number of layers' effect	
height (mm)	DF's Err	Number	DF's Err
0.32	6.7 (%)	3	1.1 (%)
0.23	6.1 (%)	5	2.1 (%)
0.1	2.9 (%)	7	1.5 (%)
0.06	1.3 (%)	9	0.5 (%)
0.02		15	

Appendix B: Particle number study

The results for DF of particles should be independent of the number of injected particles at the inlet of the computational domain. Therefore, for different particle diameters, the number of injected particles at the computational domain inlet is increased step-by-step until the changes in particle DF were negligible. The needed number of particles for the results to be independent of the number of injected particles varies with particle diameter. The smaller particles have a lower percentage of DF within the nasal cavity, and because of that, obtaining an independent result for DF requires a higher number of particles, especially for smaller surfaces. On the other hand, large numbers of injected particles also require high computational resources. In this study, diameters of 2, 10, and 30-μm were selected, and the independency of the DF percentage from the number of injected particles is investigated. The results showed that by injecting 1,400,000 2-μm particles and 260,000 10 and 30-μm particles, the changes in DF for the nasal cavity regions were, respectively, less than 2, 1.3, and 0.7 percent compared to those with a higher number of particle injection. The particles were injected from the hemispherical surface, which is the inlet of the computational domain. The graph for particle number study for 2-μm particles is shown in Fig. B. The DF is defined as the ratio of the number of deposited particles to the number of inhaled particles. A similar trend has been observed for the 10 and 30-μm size particles but with a smaller number for the needed final number of particles.
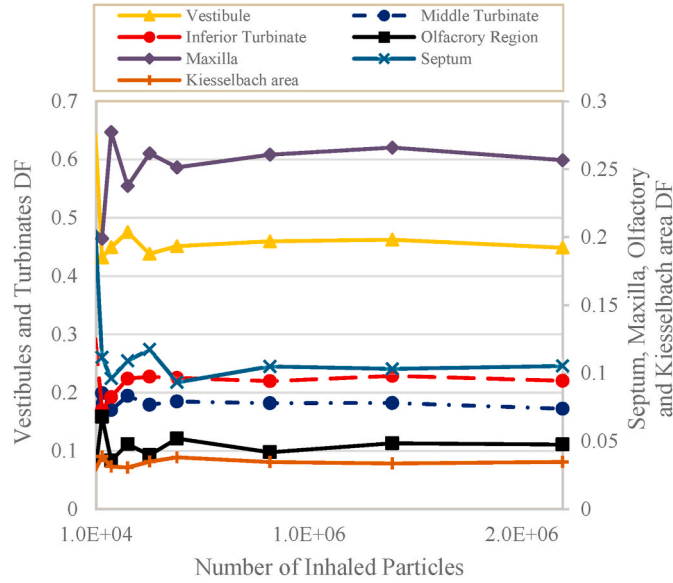
Fig. B. Number of particle study for 2-μm size particles in the nasal passage surfaces.

Appendix C: CFD-DPM method

In this study, a one-way interaction between the fluid phase and the particles is considered, which means the flow carries the particles, but the particles do not affect the flow field. Therefore, by solving the flow equations, the velocity field within the computational domain is calculated, and then the particle trajectory analysis is performed. Flow equations include the equation of conservation of mass and balance of momentum. The three dimensional, steady, incompressible and laminar forms of the governing equations for the airflow are:

$$\nabla \cdot u = 0 \tag{C-1}$$

$$\rho(u \cdot \nabla)u = -\nabla p + \mu \nabla^2 u \tag{C-2}$$

In these equations, $u = u(x.y.z)$ is the fluid velocity, p represents the static pressure and $\rho = 1.225 (\text{kg}/\text{m}^3)$ and $\mu = 1.7894 \times 10^{-5} (\text{kg}/\text{m.s})$ are, respectively, the density and viscosity of the inhaled air.

The Lagrangian approach is used to solve the Newton equations of motion for particles. The particle equation of motion is given as,

$$\frac{d\overrightarrow{u_p}}{dt} = \frac{1}{\tau} \frac{C_D Re_p}{24} \left(\overrightarrow{u} - \overrightarrow{u_p}\right) + \overrightarrow{g} \tag{C-3}$$

$$C_D = a_1 + \frac{a_2}{Re_p} + \frac{a_3}{Re_p^2} \tag{C-4}$$

$$Re_p = \frac{d_p \left| \overrightarrow{u} - \overrightarrow{u_p} \right|}{\nu} \tag{C-5}$$

$$\tau = \frac{\rho_p d_p^2}{18\mu} \tag{C-6}$$

In the above equations, $\overrightarrow{u_p}$ and $\overrightarrow{u}$ are, respectively, the particle and fluid velocity vectors, C_D is the drag coefficient defined by equation (C-4), Re_p is the particle Reynolds number defined in equation (C-5), d_p is the particle diameter and ρ_p is the density of the particle. Coefficients a_1, a_2 and a_3 are function of Re_p(S. A. Morsi and A. J. Alexander, 1972). The relaxation time is also defined by equation (C-6).

For the walls of the nasal cavity and the outer surfaces in the surrounding area, the no-slip boundary condition was assumed. At the inlet of the geometry, which is a hemispherical surface, the boundary condition of atmospheric pressure was considered, and at the outlet of the model (end of the nasopharynx), the mass flow rate boundary condition was applied (Fig. C). Two different volumetric flow rates of 125 and 250 cm^3/s (7.5 and 15 L/min) are investigated. These two flow rates represent breathing rates during rest and light daily activity conditions. The flow is assumed to be laminar in these flow rates (Wen et al., 2007).

The particle release locations are 3 mm inside the spherical surface around the face to ensure that all particles are injected inside the domain. The particles are released with a zero initial velocity from the initial locations in the surrounding volume to have a better

estimation of the location and velocity of the particles at the nares. The benefits of including the surrounding areas of the nose for a more accurate estimation of the deposition fraction of the particles in the nasal passage have been discussed in the literature (King Se, Inthavong, & Tu, 2010; Naseri et al., 2014; Hazeri, Farshidfar, Faramarzi, Sadrizadeh, & Abouali, 2020; Y. Shang, Dong, Inthavong, & Tu, 2015; Y.D. Shang, Inthavong, & Tu, 2015). For the boundary conditions of the particles, as shown in Fig. C for the surface of the face and all surfaces within the nasal cavity, the trap boundary condition was used. The outlet at the end of the nasopharynx is also given an escape boundary condition to model the penetration of the non-deposited particles into the larynx region.
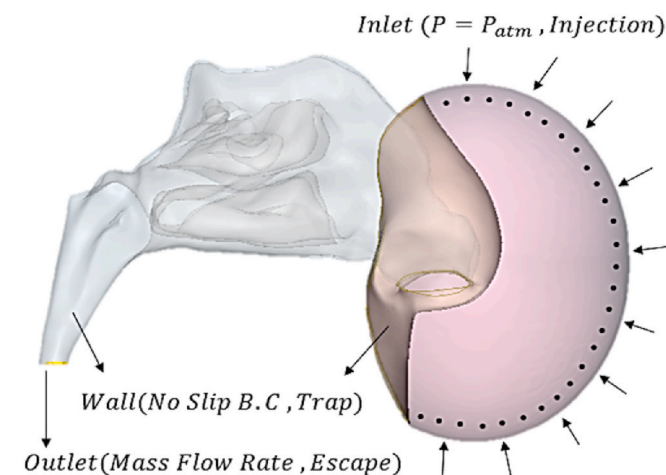

Fig. C. Boundary conditions of the flow field and particle transport equations.

Appendix D. Supplementary data

Supplementary data to this article can be found online at https://doi.org/10.1016/j.jaerosci.2020.105700.

References

Abouali, O., Keshavarzian, E., Farhadi Ghalati, P., Faramarzi, A., A, G., & B, M. H. (2012). Micro/Nano-particle deposition in maxillary sinus pre and post virtual uncienctomy. *Respiratory Physiology & Neurobiology Journal, 181*(3), 335–345.

Arthur, C., & Guyton, J. E. H. (2016). *Guyton and Hall textbook of medical physiology* (13TH ed.).

Bahmanzadeh, H., Abouali, O., & Ahmadi, G. (2016). Unsteady particle tracking of micro-particle deposition in the human nasal cavity under cyclic inspiratory flow. *Journal of Aerosol Science, 101*, 86–103. https://doi.org/10.1016/j.jaerosci.2016.07.010

Bahmanzadeh, H., Abouali, O., Faramarzi, M., & Ahmadi, G. (2015). Numerical simulation of airflow and micro-particle deposition in human nasal airway pre- and post-virtual sphenoidotomy surgery. *Computers in Biology and Medicine, 61*(March), 8–18. https://doi.org/10.1016/j.compbiomed.2015.03.015

Bear, M. F., Connors, B. W., & Paradiso, M. A. (2007). In E. Lupash (Ed.), *Neuroscience - exploring the brain* (3rd ed.). Lippincott Williams & Wilkins.

Bennett, W. D., Zeman, K. L., & Jarabek, A. M. (2008). Nasal contribution to breathing and fine particle deposition in children versus adults. *Journal of Toxicology and Environmental Health Part A: Current Issues, 71*(3), 227–237. https://doi.org/10.1080/15287390701598200

Borojeni, A. A. T., Garcia, G. J. M., Moghaddam, M. G., Frank-Ito, D. O., Kimbell, J. S., Laud, P. W., et al. (2020). Normative ranges of nasal airflow variables in healthy adults. *International Journal of Computer Assisted Radiology and Surgery, 15*(1), 87–98. https://doi.org/10.1007/s11548-019-02023-y

Borojeni, A. A. T., Noga, M. L., Vehring, R., & Finlay, W. H. (2014). Measurements of total aerosol deposition in intrathoracic conducting airway replicas of children. *Journal of Aerosol Science, 73*, 39–47. https://doi.org/10.1016/j.jaerosci.2014.03.005

Dastan, A., Abouali, O., & Ahmadi, G. (2014). CFD simulation of total and regional fiber deposition in human nasal cavities. *Journal of Aerosol Science, 69*, 132–149. https://doi.org/10.1016/j.jaerosci.2013.12.008

De Wang, Y., Lee, H. P., & Gordon, B. R. (2012). Impacts of fluid dynamics simulation in study of nasal airflow physiology and pathophysiology in realistic human three-dimensional nose models. *Clinical and Experimental Otorhinolaryngology, 5*(4), 181–187. https://doi.org/10.3342/ceo.2012.5.4.181

Djupesland, P. G. (2013). Nasal drug delivery devices: Characteristics and performance in a clinical perspective — a review. *Drug Delivery and Translational Research, 3*(1), 42–62. https://doi.org/10.1007/s13346-012-0108-9

Djupesland, P. G., Messina, J. C., & Mahmoud, R. A. (2014). The nasal approach to delivering treatment for brain diseases: An anatomic, physiologic, and delivery technology overview. *Therapeutic Delivery, 5*(6), 709–733. https://doi.org/10.4155/tde.15.92

Dong, J., Ma, J., Shang, Y., Inthavong, K., Qiu, D., Tu, J., et al. (2018). Detailed nanoparticle exposure analysis among human nasal cavities with distinct vestibule phenotypes. *Journal of Aerosol Science, 121*, 54–65. https://doi.org/10.1016/j.jaerosci.2018.05.001

Dong, J., Shang, Y., Inthavong, K., Chan, H. K., & Tu, J. (2018). Partitioning of dispersed nanoparticles in a realistic nasal passage for targeted drug delivery. *International Journal of Pharmaceutics, 543*(1–2), 83–95. https://doi.org/10.1016/j.ijpharm.2018.03.046

Dykewicz, M. S., & Hamilos, D. L. (2010). Rhinitis and sinusitis. *The Journal of Allergy and Clinical Immunology, 125*(2 SUPPL. 2), S103–S115. https://doi.org/10.1016/j.jaci.2009.12.989

Farhadi Ghalati, P., Keshavarzian, E., Abouali, O., Faramarzi, A., Tu, J., & Shakibafard, A. (2012). Numerical analysis of micro- and nano-particle deposition in a realistic human upper airway. *Computers in Biology and Medicine, 42*(1), 39–49. https://doi.org/10.1016/j.compbiomed.2011.10.005

Garcia, G. J. M., Schroeter, J. D., & Kimbell, J. S. (2015). Olfactory deposition of inhaled nanoparticles in humans. *Inhalation Toxicology, 27*(8), 394–403. https://doi.org/10.3109/08958378.2015.1066904

Garcia, G. J. M., Tewksbury, E. W., Wong, B. A., & Kimbell, J. S. (2009). Interindividual variability in nasal filtration as a function of nasal cavity geometry. *Journal of Aerosol Medicine and Pulmonary Drug Delivery, 22*(2), 139–155. https://doi.org/10.1089/jamp.2008.0713

Ghahramani, E., Abouali, O., Emdad, H., & Ahmadi, G. (2014). Numerical analysis of stochastic dispersion of micro-particles in turbulent flows in a realistic model of human nasal/upper airway. *Journal of Aerosol Science, 67*, 188–206. https://doi.org/10.1016/j.jaerosci.2013.09.004

Ghahramani, E., Abouali, O., Emdad, H., & Ahmadi, G. (2017). Numerical investigation of turbulent airflow and microparticle deposition in a realistic model of human upper airway using LES. *Computers & Fluids, 157*, 43–54. https://doi.org/10.1016/j.compfluid.2017.08.003

Gleeson, M., & Clarke, R. (2008). In R. W. C. J. C. Watkinson (Ed.), *Scott-Brown's otorhinolaryngology: Head and neck surgery 7Ed.* CRC Press.

Golshahi, L., & Hosseini, S. (2018). Intranasal filtration of inhaled aerosol in human subjects as a function of nasal pressure drop. *Journal of Aerosol Medicine and Pulmonary Drug Delivery, 32*(1), 13–23. https://doi.org/10.1089/jamp.2018.1476

Hazeri, M., Farshidfar, Z., Faramarzi, M., Sadrizadeh, S., & Abouali, O. (2020). Respiratory Physiology & Neurobiology Details of the physiology of the aerodynamic and heat and moisture transfer in the normal nasal cavity. *Respiratory Physiology & Neurobiology, 280*. https://doi.org/10.1016/j.resp.2020.103480

Jaques, P. A., & Kim, C. S. (2000). Measurement of total lung deposition of inhaled ultrafine particles in healthy men and women. *Inhalation Toxicology, 12*(8), 715–731.

Jeong, K. Y. (2016). Physical and biochemical characteristics of allergens. *Allergy, Asthma & Respiratory Disease, 4*(May), 157–166.

Keeler, J. A., Patki, A., Woodard, C. R., & Frank-Ito, D. O. (2015). A computational study of nasal spray deposition pattern in four ethnic groups. *Journal of Aerosol Medicine and Pulmonary Drug Delivery, 29*(2), 153–166. https://doi.org/10.1089/jamp.2014.1205

Kelly, J. T., Asgharian, B., Kimbell, J. S., & Wong, B. A. (2004). Particle deposition in human nasal airway replicas manufactured by different methods. Part I: Inertial regime particles. *Aerosol Science and Technology, 38*(11), 1063–1071. https://doi.org/10.1080/027868290883360

Kiasadegh, M., Emdad, H., Ahmadi, G., & Abouali, O. (2020). Transient numerical simulation of airflow and fibrous particles in a human upper airway model. *Journal of Aerosol Science, 140*, 105480. https://doi.org/10.1016/j.jaerosci.2019.105480

King Se, C. M., Inthavong, K., & Tu, J. (2010). Inhalability of micron particles through the nose and mouth. *Inhalation Toxicology, 22*(4), 287–300. https://doi.org/10.3109/08958370903295204

Leopold, D. A., Schwob, J. E., Hummel, T., Kobal, G., Knecht, M., & Hong, S. C. (1995). Anterior distribution of human olfactory epithelium. *The Laryngoscope, 110* (March), 417–421.

Liu, T., Han, D., Wang, J., Tan, J., Zang, H., Wang, T., et al. (2012). Effects of septal deviation on the airflow characteristics: Using computational fluid dynamics models. *Acta Oto-Laryngologica, 132*(3), 290–298. https://doi.org/10.3109/00016489.2011.637233

López-Elizalde, R., Campero, A., Sánchez-Delgadillo, T., Lemus-Rodríguez, Y., López-González, M. I., & Godínez-Rubí, M. (2018). Anatomy of the olfactory nerve: A comprehensive review with cadaveric dissection. *Clinical Anatomy, 31*(1), 109–117. https://doi.org/10.1002/ca.23003

Luczynska, C. M., Li, Y., Chapman, M. D., & Platts-Mills, T. A. E. (1990). Airborne concentrations and particle size distribution of allergen derived from domestic cats (*Felis domesticus*): Measurements using cascade impactor, liquid impinger, and a two-site monoclonal antibody assay for *Fel d* I. *American Review of Respiratory Disease, 141*(2), 361–367. https://doi.org/10.1164/ajrccm/141.2.361

Moran, D. T., Rowley, J. C., Jafek, B. W., & Lovell, M. (1982). The fine structure of the olfactory mucosa in man. *Journal of Neurocytology, 11*(5), 721–746, 6.

Morsi, S. A., & Alexander, A. J. (1972). An investigation of particle trajectories in two-phase flow systems. *Journal of Fluid Mechanics, 55*(2), 193–208.

Naseri, A., Abouali, O., Ghalati, P. F., & Ahmadi, G. (2014). Numerical investigation of regional particle deposition in the upper airway of a standing male mannequin in calm air surroundings. *Computers in Biology and Medicine, 52*, 73–81. https://doi.org/10.1016/j.compbiomed.2014.06.007

Naseri, A., Shaghaghian, S., Abouali, O., & Ahmadi, G. (2017). Numerical investigation of transient transport and deposition of microparticles under unsteady inspiratory flow in human airways. *Respiratory Physiology & Neurobiology, 244*, 56–72. https://doi.org/10.1016/j.resp.2017.06.005

Platts-Mills, T. A. E. (1998). The role of allergens in allergic airway disease. *The Journal of Allergy and Clinical Immunology, 101*(2 SUPPL), 364–366. https://doi.org/10.1016/s0091-6749(98)70221-0

Sahin-Yilmaz, A., & Naclerio, R. M. (2011). Anatomy and physiology of upper airway obstruction. *Proceedings of the American Thoracic Society, 8*(1), 31–39. https://doi.org/10.1016/B978-1-4160-6645-3.00101-8

Salvaggio, J. E. (1994). Inhaled particles and respiratory disease. *The Journal of Allergy and Clinical Immunology, 94*(2 SUPPL. 18), 304–309. https://doi.org/10.1053/ai.1994.v94.a56009

Schroeter, J. D., Garcia, G. J. M., & Kimbell, J. S. (2011). Effects of surface smoothness on inertial particle deposition in human nasal models. *Journal of Aerosol Science, 42*(1), 52–63. https://doi.org/10.1016/j.jaerosci.2010.11.002

Shang, Y., Dong, J., Inthavong, K., & Tu, J. (2015). Comparative numerical modeling of inhaled micron-sized particle deposition in human and rat nasal cavities. *Inhalation Toxicology, 27*(13), 694–705. https://doi.org/10.3109/08958378.2015.1088600

Shang, Y. D., Inthavong, K., & Tu, J. Y. (2015). Detailed micro-particle deposition patterns in the human nasal cavity influenced by the breathing zone. *Computers & Fluids, 114*, 141–150. https://doi.org/10.1016/j.compfluid.2015.02.020

Shi, H., Kleinstreuer, C., & Zhang, Z. (2006). Laminar airflow and nanoparticle or vapor deposition in a human nasal cavity. *Model, 128*(October 2006), 697–706. https://doi.org/10.1115/1.2244574

Suman, J. D. (2013). Current understanding of nasal morphology and physiology as a drug delivery target. *Drug Delivery and Translational Research, 3*(1), 4–15. https://doi.org/10.1007/s13346-012-0121-z

Wang, K., Denney, T. S., Morrison, E. E., & Vodyanoy, V. J. (2006). Numerical simulation of air flow in the human nasal cavity. In *2005 IEEE engineering in medicine and biology 27th annual conference. IEEE* (pp. 5607–5610). https://doi.org/10.1109/iembs.2005.1615757

Wen, J., Inthavong, K., Tian, Z., Tu, J., Xue, C., & Li, C. (2007). Airflow patterns in both sides of a realistic human nasal cavity for laminar and turbulent conditions. *16th Australasian Fluid Mechanics Conference (AFMC)*, 68–74.

Xi, J., & Longest, P. W. (2008). Numerical predictions of submicrometer aerosol deposition in the nasal cavity using a novel drift flux approach. *International Journal of Heat and Mass Transfer, 51*(23–24), 5562–5577. https://doi.org/10.1016/j.ijheatmasstransfer.2008.04.037

Xi, J., Si, X., Kim, J. W., & Berlinski, A. (2011). Simulation of airflow and aerosol deposition in the nasal cavity of a 5-year-old child. *Journal of Aerosol Science, 42*(3), 156–173. https://doi.org/10.1016/j.jaerosci.2010.12.004

Xi, J., Zhang, Z., & Si, X. A. (2015). Improving intranasal delivery of neurological nanomedicine to the olfactory region using magnetophoretic guidance of microsphere carriers. *International Journal of Nanomedicine, 10*, 1211–1222.

Xi, J., Zhang, Z., Si, X. A., Yang, J., & Deng, W. (2016). Optimization of magnetophoretic-guided drug delivery to the olfactory region in a human nose model. *Biomechanics and Modeling in Mechanobiology, 15*(4), 877–891. https://doi.org/10.1007/s10237-015-0730-9

Zhao, K., & Jiang, J. (2014). What is normal nasal airflow? A computational study of 22 healthy adults. *International Forum of Allergy and Rhinology, 4*(6), 435–446. https://doi.org/10.1002/alr.21319

Zhao, K., Jiang, J., Pribitkin, E. A., Dalton, P., Rosen, D., Lyman, B., et al. (2014). Conductive olfactory losses in chronic rhinosinusitis? A computational fluid dynamics study of 29 patients. *International Forum of Allergy and Rhinology, 4*(4), 298–308. https://doi.org/10.1002/alr.21272

Zhu, J. H., Lee, H. P., Lim, K. M., Lee, S. J., & Wang, D. Y. (2011). Evaluation and comparison of nasal airway flow patterns among three subjects from Caucasian, Chinese and Indian ethnic groups using computational fluid dynamics simulation. *Respiratory Physiology & Neurobiology, 175*(1), 62–69. https://doi.org/10.1016/j.resp.2010.09.008